Available online at www.sciencedirect.com
ScienceDirect
Journal of the European Ceramic Society 28 (2008) 1953–1960
www.elsevier.com/locate/jeurceramsoc

Microstructural changes and evolutions of elastic properties versus temperature of alumina and alumina–magnesia refractory castables

Jean-Michel Auvray [a], Christian Gault *, Marc Huger

Groupe d'Etude des Matériaux Hétérogènes (GEMH), ENSCI, 47 à 73 Avenue Albert Thomas, 87065 Limoges, France

Received 28 November 2007; received in revised form 5 February 2008; accepted 8 February 2008
Available online 15 April 2008

Abstract

This paper deals with the evolutions of thermo-mechanical properties of castable refractories versus temperature. The measured properties are mainly Young's modulus evaluated by a high temperature ultrasonic technique and thermal expansion followed by dilatometry. Materials are alumina-based low cement castables with a fraction of alumina eventually substituted by spinel or magnesia. The granularity of the different used raw materials is chosen by using a packing model, in order to reduce the final porosity in the hydrated state. The interpretation of results is carried out by considering the materials as composites, constituted of aggregates (size > 100 μm) into a matrix where most of chemical and phase transformations occur. By using two-phase analytical models, it is shown that the evolutions of thermo-elastic properties of castables can be qualitatively predicted from measurements performed in a matrix-equivalent simplified material. Moreover, considering the elastic properties after heat treatment, the castable with magnesia is comparable to the castable processed with synthetic spinel.

Keywords: Refractory castables; Ultrasonic pulse-echo; Elasticity; $MgAl_2O_4$; MgO

1. Introduction

In steel industry, there is a trend to increase the use of high-alumina refractory castables containing spinel $MgAl_2O_4$, because of their higher refractoriness and of their better corrosion resistance than Al_2O_3 castables.[1] Nevertheless, the cost of such materials is high, because synthetic spinel powders are expensive. Then, it is interesting to study alumina–magnesia castables which can develop a spinel phase during heating at high temperature. Moreover, these materials are known to present an improved temperature behaviour because of the higher densification of the Al_2O_3–MgO bonding phase after thermal treatment.[2]

Castables can be considered as composites, with the bonding phase being the matrix and aggregates being reinforcement particles.[3] Properties of the concretes at high temperature are strongly dependent upon microstructural evolutions and reactions between constituents in the matrix. In a recent paper, the high temperature behaviour of matrices of two castables, one containing alumina and another containing alumina and magnesia referred MatA and MatAM, respectively, has been studied by the way of ultrasonic measurements of elastic modulus at high temperature.[4] The matrices were constituted of a mix of the hydraulic cement and of the finest powders used for concrete fabrication, conventionally having diameters lower than 100 μm. Above this arbitrary threshold value, particles become part of the aggregate phase of concretes. Young's modulus was measured versus temperature up to 1550 °C using a specific ultrasonic pulse-echo technique and results were correlated to microstructural and phase changes. It has been shown that, during heating, the reactive alumina reacts with calcium aluminates of cement or magnesia to produce high refractoriness

* Corresponding author. Tel.: +33 5 55 45 22 35; fax: +33 5 55 79 09 98.
E-mail address: christian.gault@unilim.fr (C. Gault).
[a] Now at: KERNEOS Aluminates Technologies, 95 rue du Montmurier, ZI Parc de Chesnes, 38291 Saint-Quentin Fallavier, France.

0955-2219/$ – see front matter © 2008 Elsevier Ltd. All rights reserved.
doi:10.1016/j.jeurceramsoc.2008.02.012

Table 1
Chemical compositions and physical characteristics of raw materials

	Chemical analysis (wt%)							Physical properties		Commercial reference
	CaO	Al_2O_3	Na_2O	SiO_2	Fe_2O_3	MgO	Cl	Specific surface area (m^2/g)	Bulk density	
Cement	27.00	72.00	0.25	0.30	0.15	0.20	0.00	1.66	3.04	CA14M†
Reactive alumina	0.02	99.80	0.08	0.03	0.02	0.09	0.00	3.00, 7.00	3.91	CL370C†, CT3000SG†
Spinel	0.24	77.00	0.08	0.10	0.07	22.50	0.00	1.21	3.47	AR78†
Magnesia	0.40	0.01	0.00	0.00	0.01	98.10	1.23	6.40	3.03	Ankermag B20‡

† From Almatis.
‡ From Magnifin.

components, which are associated with changes of microstructure and mechanical properties. Important results have been obtained:

- At low temperature, mechanical properties decrease because of the dehydration process associated with volume shrinkage of hydrates.
- At 1100 °C, mono-aluminate of calcium CA[b] reacts with alumina to form di-aluminate of calcium CA_2 (see footnote b) in parallel with a volume expansion of the material. In the case of Al_2O_3–MgO–CaO system, alumina also reacts with magnesia to form in situ spinel MA (see footnote b) associated with an additional thermal expansion.[5,6] Both reactions are responsible for the enhancement of the microstructure and for the improvement of thermo-mechanical properties.
- At 1450 °C, CA_2 reacts with reactive alumina to form hexa-aluminate of calcium CA_6 (see footnote b) resulting in a porous network of interlocked platelets. For the MgO material, the higher mechanical properties can be explained by the presence of strong bond linkage between the in situ spinel grains and CA_6.

In the continuation of these results obtained for matrices, the work reported in this paper, is devoted to investigate correlations between microstructural changes and elastic properties of two concretes, termed CastA and CastM, with bonding phases corresponding to the previously studied matrix compositions MatA and MatAM during heat treatments. Additionally, a Al_2O_3–$MgAl_2O_4$ concrete, referred CastS, has been studied in order to compare its properties to that of CastM where $MgAl_2O_4$ is formed in situ at high temperature.

2. Experimental procedure

Raw materials used for the fabrication of the three concretes are: a calcium aluminate cement (CA14M, 72% Al_2O_3), reactive alumina powders (CT3000SG and CL370C, 99.8% Al_2O_3), a synthetic spinel (AR78, 77% Al_2O_3) and magnesia (Ankermag B20, 98.1% MgO). Some characteristics are summarised in Table 1. As previously explained,[4] an arbitrary threshold value has been chosen to distinguish the matrix (particles size ≤ 100 μm) from the aggregates (particles size > 100 μm). The granular skeleton of concretes is constituted of coarse aggregates of tabular alumina (T60, d_{50} from 0 to 5 mm from Almatis). For such low cement castables (LCCs), where the content of water is minimised, and in order to obtain a maximum density, the particle size distribution (PSD) has been optimised by the way of the packing model proposed by Dinger and Funk[7]:

$$\mathrm{CPFT}\,(\%) = 100 \times \left(\frac{D^q - D_S^q}{D_l^q - D_S^q} \right) \quad (1)$$

where CPFT is the so-called "cumulative percent finer than" (in volume), D is the particle size, D_S is the smallest particle size, D_l is the largest particle size and q an adjustable coefficient depending on the granular distribution.

For our systems, an exponent q of 0.25 was found to be efficient to both obtain a good casting consistency and to achieve the highest degree of compaction for concretes. Therefore, according to this law of maximum packing, the concrete formulations were obtained by adjusting the mass ratio of each component, taking care to keep an equivalent particle size distribution for all castables (see Fig. 1). Table 2 gives the wt% compositions of the three concretes. CastA is a high-alumina castable consisting in 5.4 wt% cement and 94.6 wt% Al_2O_3; it will be considered as a reference. CastS is an Al_2O_3-spinel castable containing 12 wt% synthetic spinel and CastM, is obtained by replacing 3 wt% reactive alumina in CastA by 3 wt% MgO.

The processing route for casting and curing the castables has been described in Ref. 4. For the casting of CastM, it can be noted that magnesia powder was subjected to a pre-thermal treatment at 900 °C in order to reduce its reactivity with water. After casting at room temperature, the specimens undergo a thermal

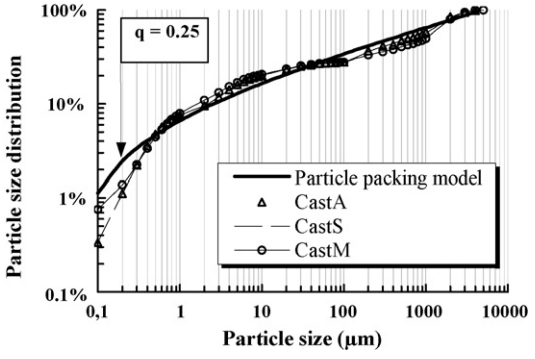

Fig. 1. Particle size distributions of the optimised formulations of the castables based on the Funk–Dinger's model (q = 0.25).

[b] Cement notations: CaO–Al_2O_3 = CA; CaO–$2Al_2O_3$ = CA_2; CaO–$6Al_2O_3$ = CA_6; MgO–Al_2O_3 = MA.

Table 2
Compositions of castables (wt%)

Materials	CastA	CastS	CastM
Cement CA14M	5.40	5.40	5.40
Reactive alumina			
CT3000SG	3.80	3.80	2.60
CL370C	10.20	10.20	8.40
Tabular alumina T60			
45 μm	3.80	3.80	3.80
0–1 mm	28.80	11.80	15.70
0–3 mm	3.00	6.00	8.70
0–5 mm	27.00	29.00	32.40
1–2 mm	18.00	18.00	20.00
Spinel AR78	0.00	12.00	0.00
Magnesia	0.00		3.00
Water	5.00	5.00	5.50

treatment, which consists in heating at 110 °C for 48 h before characterisation.

Bulk density and apparent porosity of specimens were measured by the Archimedes method in water (containing a wetting agent). Microstructures of sample fractures were examined by using scanning electron microscopy (SEM).

Thermal expansion measurements were performed at 5 °C/min from room temperature to 1500 °C in samples of dimensions 20 mm × 8 mm × 8 mm, using an horizontal 1500 °C dilatometer (ADAMEL DI24).

Measurements of the elastic modulus E of the specimens were achieved via a high temperature ultrasonic technique shown in Fig. 2, whose principle was already reported.[4,8] The value of Young's modulus of the material is obtained from the measurement of the time delay τ between two successive echoes in the sample. The characteristics of the different parts of the ultrasonic line have been adapted to the highly heterogeneous refractory concretes with large grains (up to 5 mm) and high porosity (up to 15%), which involve a high ultrasonic attenuation: the dimensions of samples and the wave frequency are 80 mm × 20 mm × 20 mm and 110 kHz, respectively. Experiments have been performed during a thermal treatment consisting in heating/cooling rates of 5 °C/min from room temperature to 1550 °C, with a dwell at 1550 °C for 2 h.

Table 3
Microstructural characteristics and elastic modulus of castables after thermal treatment at 110, 400 and 1550 °C

Material	Density/porosity (%)			Young's modulus (GPa)		
	110 °C	400 °C	1550 °C	110 °C	400 °C	1550 °C
CastA	3.13/12.9	3.09/16.35	3.08/17.8	80	41	117
CastS	3.12/12.8	3.09/16.3	3.10/17.5	74	40	123
CastM	3.12/12.5	3.07/15.8	3.01/19	83	37	112

3. Results and discussion

Density, porosity and Young's modulus have been determined at room temperature after treatments at 110, 400 and 1550 °C. The results are summarised in Table 3. The three castables exhibit similar characteristics in the as-cured state and similar trends after heat treatments:

- A decrease of stiffness and an increase of porosity after treatment at 400 °C.
- An increase of elastic modulus and an increase of porosity after treatment at 1550 °C.

Figs. 3 and 4 show thermal expansions and Young's modulus variations measured during thermal cycles at 5 °C/min from room temperature to 1550 °C for the three materials.

3.1. Variations observed during the thermal cycle

Five stages can be distinguished on the curves, with similar trends for the three materials, but with a rather significant difference for CastM compared to CastA and CastS.

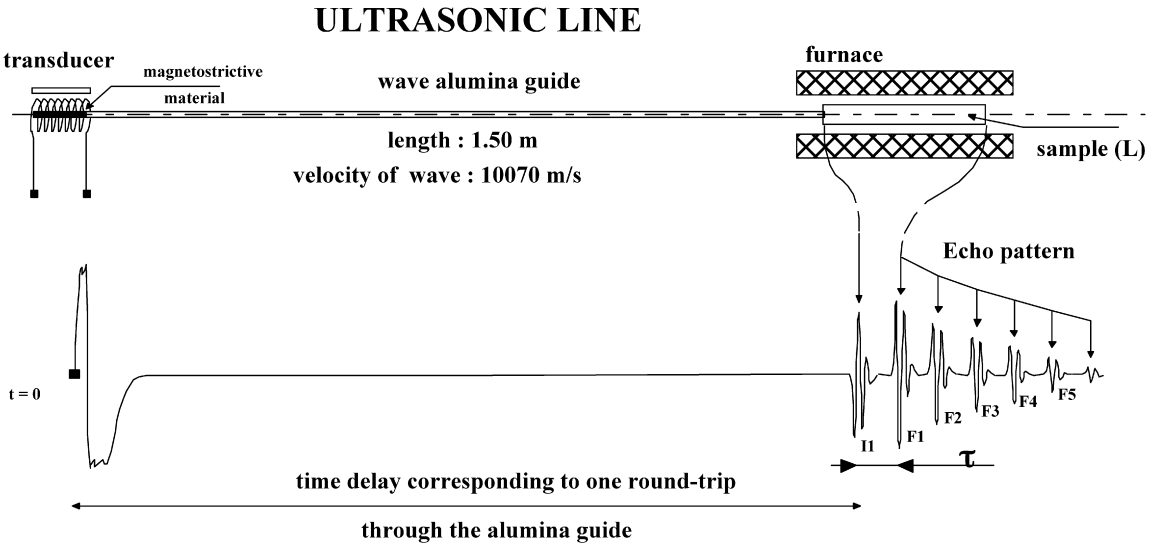

Fig. 2. Principle of ultrasonic Young's modulus measurements at high temperature.

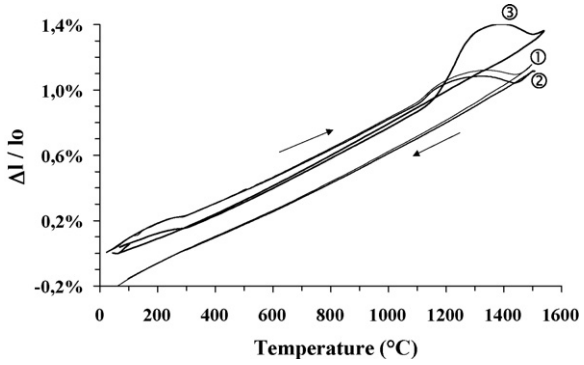

Fig. 3. Thermal expansion of castables vs. temperature. Curve ①: CastA; curve ②: CastS; curve ③: CastM.

Table 4
Wt% compositions and solid volume of phases as function of temperature for the reference castable CastA

	Phases			
	A	CA	CA_2	CA_6
Mass (wt%) at				
1000 °C	95.125	3.75	1.125	0
1250 °C	92.75	0	7.25	0
1550 °C	81.375	0	0	18.625
Solid volume (%) at				
1000 °C	93.875	4.675	1.45	0
1250 °C	91	0	9	0
1550 °C	80.625	0	0	19.375

3.1.1. From room temperature to 400 °C

Between 200 and 400 °C, Young's modulus exhibits a strong decrease of approximately 50% from the value measured at room temperature and a very slight shrinkage is observed (about 0.1% in Fig. 3), associated with a small increase of the apparent porosity (from 13 to 16% in Table 3). The comparison to results of similar experimentations in matrices[4] suggests that these effects are linked to dehydration of the cementitious phases.

3.1.2. From 400 to 1100 °C

The thermal expansion and $E = f(T)$ curves do not exhibit any noticeable effect, as well as previously observed for matrices.[4] The dehydrated materials have very low Young's modulus (35–40 GPa). Thermal expansion is approximately linear and reversible and corresponds to a coefficient of thermal expansion (CTE) of $8.9 \times 10^{-6}\,°C^{-1}$ close to that of Al_2O_3.

3.1.3. From 1100 to 1300 °C

At 1100 °C, dilatometry curves exhibit an expansion (Fig. 3) attributed to the expansive formation of CA_2 for the Al_2O_3 and spinel castables (CastA and CastS, respectively) and, in the case of CastM, to the expansive formation of both CA_2 and in situ spinel MA. Based on the chemical composition of the reference castable CastA (see Table 4), the variation of the theoretical solid volume of the material after formation of CA_2 was estimated to 3.05% (see Table 5) which is one order of magnitude superior to the measured expansion. This difference can be attributed to a partial resorption of matrix porosity, associated with the expansive formation of CA_2. In the same temperature range, the Young's modulus of materials exhibits a sharp increase, which denotes the stiffening of the microstructure. This effect has been observed in matrices,[4] but seems to be more important for castables than this expected for the corresponding fractional volume of matrix.[3] It can be deduced that, even if the amount of formed CA_2 or/and spinel phases is lower for concretes than for matrices, the associated expansive effect, added with the beginning of sintering, are efficient to heal the microcracks at the aggregates–matrix interfaces.[9] By this way, the higher improvement of elastic properties in the case of CastM can be explained by the higher value of the thermal expansion associated with the in situ formation of spinel.

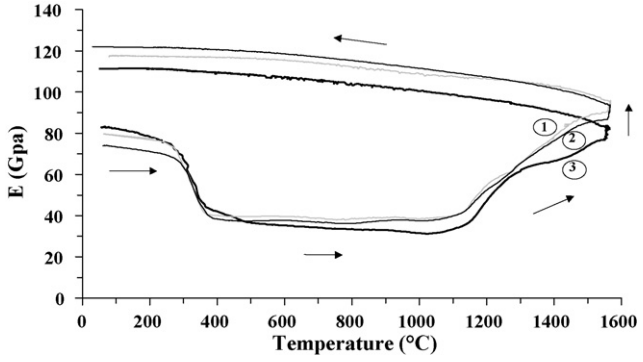

Fig. 4. Evolutions of elastic modulus of castables vs. temperature. Curve ①: CastA; curve ②: CastS; curve ③: CastM.

3.1.4. From 1300 to 1450 °C

With increasing temperature, the densification by sintering results in a shrinkage of castables, in parallel with a regular and monotonic growth of elastic modulus. It must be noted that the stiffening rate of CastM is lower than for the two others, which could be explained by a significant amount of viscous phase coming from MgO impurities.[3]

3.1.5. From 1450 to 1550 °C

The trend to shrinkage by densification of the materials is opposed to the expansive formation of hexagonal platelets of CA_6, associated with an increase of porosity. The consequence is a slowdown of the increasing rate of elastic modulus versus temperature, which becomes effective at 1450 °C. Furthermore, for the MgO castable, this phenomenon is more attenuated and occurs at a higher temperature (about 1500 °C) than for CastA

Table 5
Volume expansions as function of temperature for the reference castable CastA based on the wt% compositions (Th.), expected from results obtained for the corresponding Al_2O_3 matrix (Cal.) and from experiments (Exp.)

Phenomenon	$\Delta V/V$ (%)		
	Th.	Cal.	Exp.
CA_2 (1100–1250 °C)	+3.05	+0.16	+0.18
Sintering (1000–1450 °C)		−1.90	−0.60
CA_6 (1450–1550 °C)	+1.50		>0.33

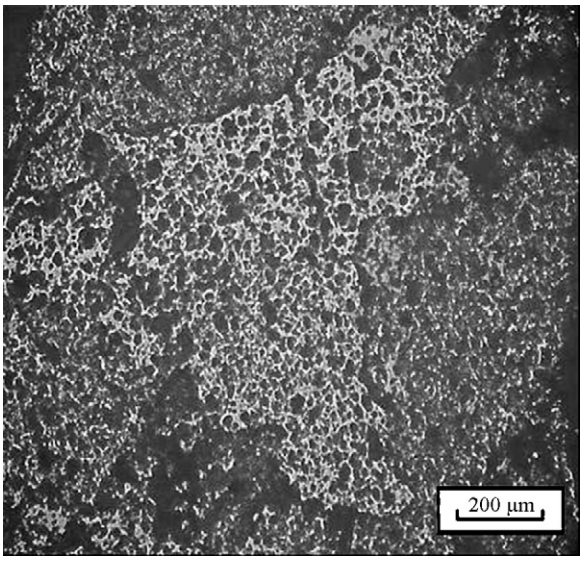

Fig. 5. Microstructure observations by optical microscopy of the reference castable CastA treated at 1550 °C.

and CastS. It suggests that at this temperature, sintering of MgO is the dominant mechanism, probably promoted by a viscous phase. This could explain the better resistance to slag of this type of castable compared to single alumina castables. During the dwell at 1550 °C, the increase of elastic modulus is attributed to the densification by sintering of the materials. Actually, the observation of CastA heated at 1550 °C reveals a uniformly dense microstructure (Fig. 5).

On cooling, the regular increase of elastic modulus observed on the curves of Fig. 4 is characteristic of stable and dense materials.[10] SEM observations (Fig. 6) reveal the bonding between the matrix and the aggregate phase. Fig. 6b illustrates the development of CA_6 inside a tabular alumina grain. Finally, at room temperature, the values of elastic modulus of the three materials after heat treatment at 1550 °C are similar (within 10%). Thus, considering the elastic properties, the MgO castable with 3 wt% magnesia can be comparable with the 12 wt% synthetic spinel castable.

3.2. Quantitative comparison between matrix and concrete behaviours

Most effects, in particular dehydration and densification at high temperature appear to be similar in matrix and concrete. Then, an attempt is made in this section to quantify, by the way of two-constituent composite models applied to the reference castable CastA, the impact of the proper effect of the matrix on the evolutions versus temperature of thermal expansion and of Young's modulus.

The composite is assumed to be constituted from a continuous matrix MatA, previously studied in Ref. 4 and a discrete phase, alumina aggregates, supposed to be inert during heat treatment. From the composition of CastA given in Table 2, the fractional volumes v_m and v_a for matrix and aggregates were found to be 38 and 62%, respectively.[3] Thermal and elastic properties of aggregates are reported for tabular alumina in Ref. 11.

3.2.1. Thermal expansion

The calculation of thermal expansion of a two-phased composite must take into account the interaction between phases of different CTE, which induces internal stresses. For non-linear thermal expansion, which is the case of the matrix and of the concrete where microstructural transformations occur with temperature changes, the CTE at a given temperature T, $\alpha(T)$ is defined in Fig. 7.

According to the thermo-elastic model of Fahmy and Ragai[12] $\alpha(T)$ can be calculated for the concrete by the following equation:

$$\alpha(T)=\alpha_m-\left[\frac{3(\alpha_m-\alpha_a)(1-\nu_m)v_a}{(2E_m/E_a)(1-2\nu_a)v_m+2v_a(1-2\nu_m)+(1+\nu_m)}\right] \quad (2)$$

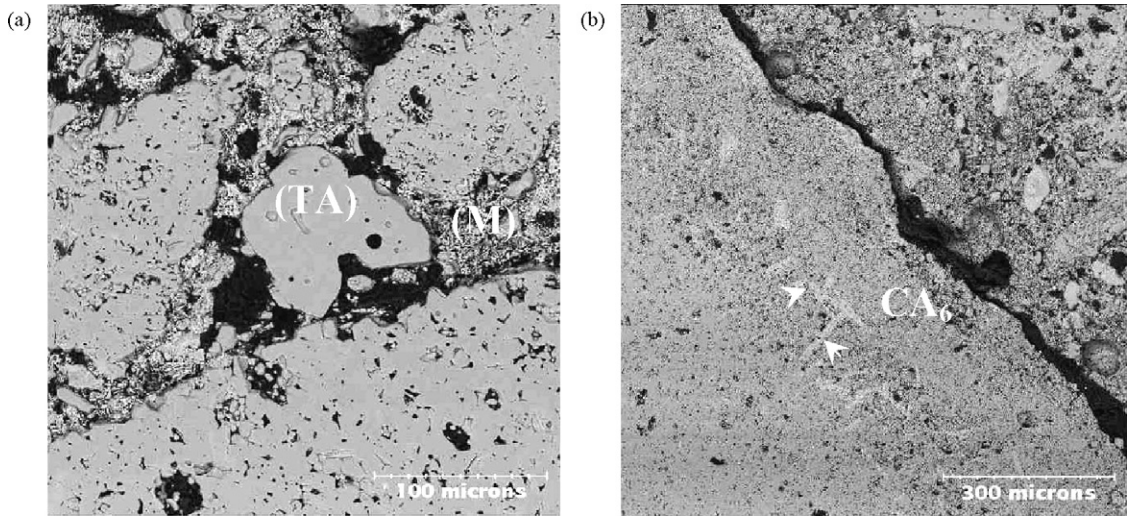

Fig. 6. Backscattered electron imaging (BSI) microstructures of CastA, heated at 1550 °C, revealing the bond linkage between tabular alumina grains, TA and matrix, M (a) and the growing of CA_6 grains into tabular alumina aggregates (b).

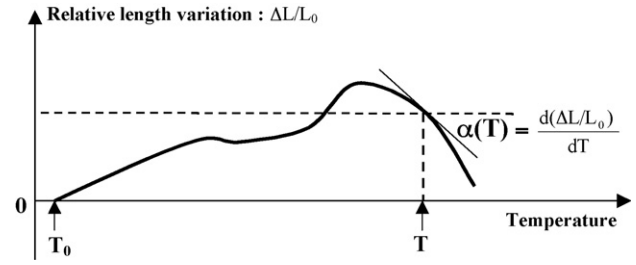

Fig. 7. Definition of the true CTE $\alpha(T)$ at a given temperature T for a non-linear thermal expansion material.

where α_a, υ_a, ν_a, E_a and α_m, υ_m, ν_m, E_m are the CTE, the fractional volume, the Poisson's ratio and Young's modulus of aggregates and matrix, respectively.

In this equation, CTE and Young's moduli depend on temperature. Poisson's ratios have been considered constant by making the approximation $\nu_m \approx \nu_a \approx 0.25$. Then it gives for CastA:

$$\alpha(T) \approx \alpha_m(T) - \frac{1.42[\alpha_m(T) - \alpha_a(T)]}{0.37(E_m(T)/E_a(T)) + 1.88} \quad (3)$$

The curve ③ in Fig. 8 shows the result of the thermal expansion of the composite calculated from Eq. (3) by taking the results of variations versus temperature of Young's modulus and of thermal expansion from Ref. 4 for the matrix (curve ② in Fig. 8) and from Ref. 11 for tabular alumina. There is a qualitative agreement compared to the experimental result (curve ①). Moreover, at room temperature, E_m is rather low (20 GPa), compared to E_a (350 GPa) and, whatever the considered temperature, the ratio E_m/E_a remains inferior to 0.3 during the thermal treatment. Consequently, Eq. (3) shows that the thermal expansion of the composite is mainly controlled by the aggregates. The large dilatometric effects observed in the matrix during dehydration of the cement ($T > 200\,°C$) and during crystallisation of new phases and sintering at high temperature ($T > 1100\,°C$) are smoothed in the concrete, both due to the low volume fraction of matrix and to the high stiffness of aggregates. Anyway, the calculated curve leads to amplitudes of variations superior to the experimental ones, in particular during dehydration and sintering stages. This could be explained by the fact that, in the concrete, one part of the matrix shrinkage is transformed into porosity.

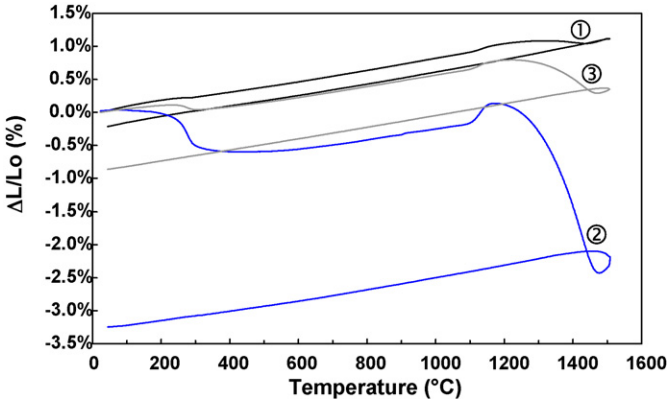

Fig. 8. Comparison between the thermal expansion obtained for the reference castable CastA and the one calculated from results obtained for its matrix MatA: ① castable, ② matrix, ③ calculated.

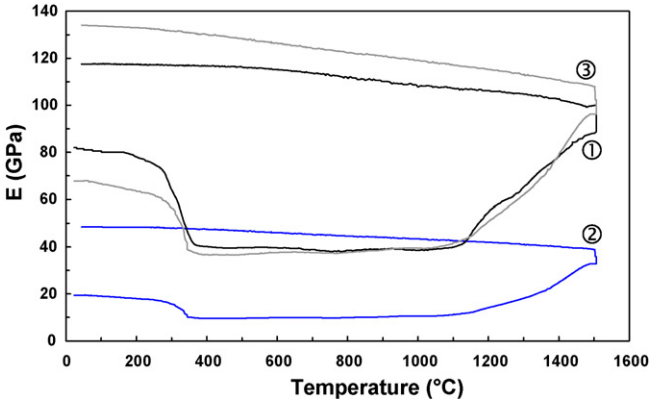

Fig. 9. Comparison between the variations in elastic modulus obtained for the reference castable CastA and those calculated from results obtained for its matrix MatA: ① castable, ② matrix, ③ calculated.

3.2.2. Young's modulus

Numerous models exist in literature for the prediction of Young's modulus of two-phased materials.[11,13–15] Most of them lead to equations corresponding to upper and lower bounds between which the true value of the modulus of the material should be located. It must be noted that these analyses assume that particles are embedded into a homogeneous matrix with perfectly adhesive interfaces. For model refractories, without debonding between matrix and aggregates, the experimental value of Young's modulus has been found to correspond to the lower bounds.[16] In the present case, a calculation of the Young's modulus has been performed with the lower bounds $(E_{HS})^-$, of the so-called Hashin–Shtrikman analysis,[15] as a function of the Young's moduli, Poisson's ratios and fractional volumes, E_m, E_a, ν_m, ν_a, υ_m and υ_a of the matrix and aggregates, respectively:

$$(E_{HS})^- = f(E_m, E_a, \nu_m, \nu_a, \upsilon_m, \upsilon_a) \quad (4)$$

The numerical calculation procedure of the f function versus temperature from the variations of E in the matrix and in alumina aggregates is detailed in Appendix A.

The result of calculation of $(E_{HS})^-$ is plotted in Fig. 9 (curve ③). For discussion, the experimental curves $E(T)$ for CastA (curve ①) and $E_m(T)$ for MatA (curve ②) are plotted on the same figure.

Several observations arise from the analysis of Fig. 9:

1. The value at RT calculated in the cured state (70 GPa) is rather close to the experimental one (80 GPa). The difference could come from the fact that the material MatA in Ref. 4 and the real matrix of CastA within the whole castable could not be exactly the same, because of processing conditions.
2. The calculated relative amplitude of decrease of Young's modulus attributed to dehydration between 200 and 400 °C is only ∼33% compared to ∼50% experimentally observed. Simonin et al.[17] attributed this difference to some microcracks between matrix and aggregates responsible for the decrease of stiffness. Actually, an observation by optical

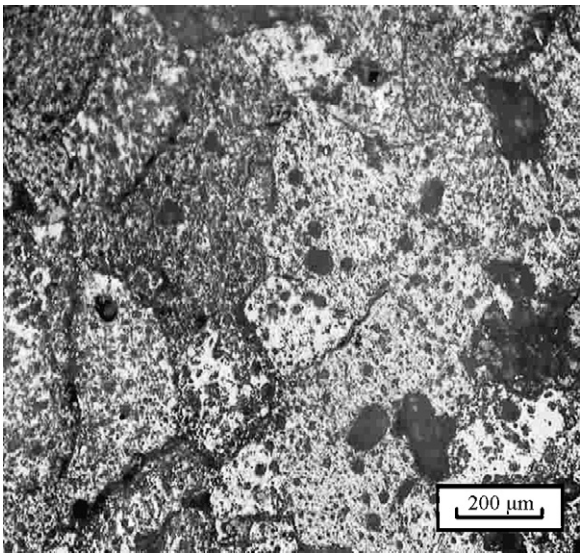

Fig. 10. Microstructure observation by optical microscopy of the dehydrated castable CastA (at 400 °C).

microscopy of the dehydrated castable CastA at 400 °C reveals the presence of such interfacial microcracking (Fig. 10).

3. All phenomena responsible for variations of Young's modulus in the matrix give analogous results in castable, but with different amplitudes of variations. In particular sintering and crystallisation of new phases above 1100 °C involve a strong increase of stiffness. At room temperature after treatment at 1550 °C, the relative increase of calculated E compared to the as-cured state is approximately ∼100% compared to the experimental value which is much lower (∼45%). This could be explained by the effect of decohesions which occur in the real material, because of volume variations associated to phase changes at high temperature and sintering effects which cannot be taken into account by the model.

4. Conclusions

The measurement of Young's modulus is well suited to follow in situ the chemical and microstructural evolutions of castables during a thermal treatment. The elastic behaviours of the three types of castables appear to be directly reliable to those observed for their bonding phases (so-called the matrix). From calculations performed by using a two-phase composite analytical model, it has been shown that the evolution of elastic properties of castables can be qualitatively predicted from measurements performed in a matrix-equivalent simplified material.

During the dehydration process, the chemical shrinkage of hydrates involves a strong decrease of elastic properties of the castables indirectly attributed to the increase of porosity and the development of microcracking.

Thermal expansion and elasticity measurements reveal a difference between the MgO castable and the other types when the formation of in situ spinel occurs at 1100 °C.

At high temperatures, the expansive formations of CA_2 and/or in situ spinel are associated to a significant increase of the elastic properties due to improvement of the grain–grain contacts between the matrix and aggregates. SEM observations reveal that some CA_6 crystals have grown inside the alumina aggregate. Moreover, the bond linkage between the CA_6 crystals and in situ spinel grains observed in the matrix can explain the important stiffness enhancement of castables with spinel or magnesia.

Acknowledgements

The authors would like to express their gratitude towards the Vesuvius Company and the Région Limousin for their financial support of the present work.

Appendix A

By using a variational approach, Hashin and Shtrikman derive upper and lower bounds for the bulk and shear moduli, K and G, of composite constituted of particles into an infinite homogeneous matrix.[15] When the stiffness of the particles is much greater than that of the matrix, which corresponds to the present case, lower bounds give a satisfactory evaluation of the experimental value of the elastic properties of the composite.

K and G are related to the Young's modulus E via the Poisson's ratio ν by

$$K = E[(1-2\nu)3]^{-1} \quad \text{and} \quad G = E[(1+\nu)2]^{-1} \tag{5}$$

By making the approximation $\nu_m \approx \nu_a \approx 0.25$, the values of K and G at a temperature T can be calculated from the variations of E versus temperature found in literature for the matrix MatA[4] and for aggregates assumed to be tabular alumina.[11]

Then, the lower bounds of bulk and shear moduli of the composite have been calculated at temperature T with the Hashin–Shtrikman equations:

$$(K_{HS})^- = K_m + \frac{v_a}{(1/(K_a - K_m)) + (3v_m/(3K_m + 4G_m))} \tag{6}$$

$$(G_{HS})^- = G_m + \frac{v_a}{(1/(G_a - G_m)) + (6(K_m + 2G_m)v_m/ 5G_m(3K_m + 4G_m))} \tag{7}$$

where suffixes 'm' and 'a' are related to matrix and aggregates, respectively.

Then the lower bound of Young's modulus of the composite at temperature T has been obtained by substitution of $(K_{HS})^-$ and $(G_{HS})^-$ and combining the two Eq. (5):

$$(E_{HS})^- = \frac{9(K_{HS})^-(G_{HS})^-}{3(K_{HS})^- + (G_{HS})^-} \tag{8}$$

References

[1]. Naaby, H., Abildgarrd, O., Stallmann, G., Wohrmeyer, C. and Meidell, J., Refractory wear mechanism and influence on metallurgy and steel quality as result of the conversion to endless lining at Det Danske Stalvalsevaerk. *Stahl und Eisen Special*. Verlag Stahleisen GmbH, Düsseldorf, 1994, pp. 198–204.

2. Ko, Y. C., Effect of compositional variables on the properties of alumina–magnesia castables. *Interceram*, 2000, **49**(5), 316–325.
3. Auvray, J. M., *Elaboration et caractérisation à haute température de bétons réfractaire à base d'alumine et de spinelle, Thesis*. Limoges University, France, 2003.
4. Auvray, J. M., Gault, C. and Huger, M., Microstructural changes and evolutions of elastic properties versus temperature in bonding phases of alumina and alumina–magnesia refractory castables. *J. Eur. Ceram. Soc.*, 2007, **27**(12), 3489–3496.
5. Xing, C., Kovac, V. and Rigaud, M., Volume stability of various $MgO–Al_2O_3$ castable mixes. *J. Can. Ceram. Soc.*, 1997, **66**(3), 217–222.
6. Fuhrer, M., Hey, A. and Lee, W., Microstructural evolution in self-forming spinel-calcium aluminate castable refractories. *J. Eur. Ceram. Soc.*, 1998, **18**, 813–820.
7. Dinger, D. R. and Funk, J. E., Particle packing. II. Review of packing of polydisperse particle systems. *Interceram*, 1992, **41**(2), 95–97.
8. Huger, M., Fargeot, D. and Gault, C., High-temperature measurement of ultrasonic wave velocity in refractory materials. *High Temp. High Press.*, 2002, **34**, 193–201.
[9]. Case, E. D., Smyth, J. R. and Hunter Jr., O., Microcraking in large-grain Al_2O_3. *Mater. Sci. Eng.*, 1981, **51**, 175–179.
10. Gault, C., Ultrasonic non destructive evaluation of microstructural changes and degradation of ceramics at high temperature. *Am. Mater. Res. Symp. Proc.*, 1989, **142**, 263–274.
11. Tessier-Doyen, N., *Etude expérimentale et numérique du comportement thermomécanique de matériaux réfractaires modèles, Thesis*. Limoges University, France, 2003.
12. Fahmy, A. A. and Ragai, A. N., Thermal-expansion behaviour of two-phase solids. *J. Appl. Phys.*, 1970, **41**(13), 5108–5111.
13. Voigt, W., *Lehrbuch der kristallphysik*. Teubner, Berlin, 1910.
14. Reuss, A., Berechnung der fliessgrenze von mischkristallen auf grund der plastizitätsbedingung für einkristallen. *Z. Angew. Math. U. Mech.*, 1929, **9**(1), 49–58.
15. Hashin, Z. and Shtrikman, S., A variational approach to the theory of the elastic behavior of multiphase materials. *J. Mech. Phys. Solids*, 1963, **11**, 127–140.
16. Tessier-Doyen, N., Glandus, J. C. and Huger, M., Untypical Young's modulus evolution of model refractories at high temperature. *J. Eur. Ceram. Soc.*, 2006, **26**(3), 289–295.
17. Simonin, F., Olagnon, C., Maximilien, S. and Fantozzi, G., Thermomechanical behavior of high-alumina refractory castables with synthetic spinel additions. *J. Am. Ceram. Soc.*, 2000, **83**(10), 2481–2490.